High-flux Robust Ceramic Membranes Functionally Decorated with Nano-Catalyst for Emerging Micro-pollutant Removal from Water

Xueling Wang[a], *Youling Li*[a], *Hongtao Yu*[a], *Fenglin Yang*[a], *Chuyang Y. Tang*[b], *Xie Quan*[*a], *Yingchao Dong*[*a]

[a] Key Laboratory of Industrial Ecology and Environmental Engineering (Ministry of Education, MOE), School of Environmental Science and Technology, Dalian University of Technology, Dalian, Liaoning Province, China 116024

[b] Department of Civil Engineering, The University of Hong Kong, Pokfulam, Hong Kong, China

Note: Xueling Wang and Youling Li made the equal contribution to this work.

Corresponding authors:

Professor Xie Quan

Key Laboratory of Industrial Ecology and Environmental Engineering (Ministry of Education, MOE), School of Environmental Science and Technology, Dalian University of Technology, Dalian, Liaoning Province, China 116024

Tel: +86-411-84706140 E-mail: quanxie@dlut.edu.cn.

Professor Yingchao Dong

Key Laboratory of Industrial Ecology and Environmental Engineering (Ministry of Education, MOE), School of Environmental Science and Technology, Dalian University of Technology, Dalian, Liaoning Province, China 116024

Tel: +86-411-84706328 E-mail: ycdong@dlut.edu.cn.

30 **Graphical abstract**

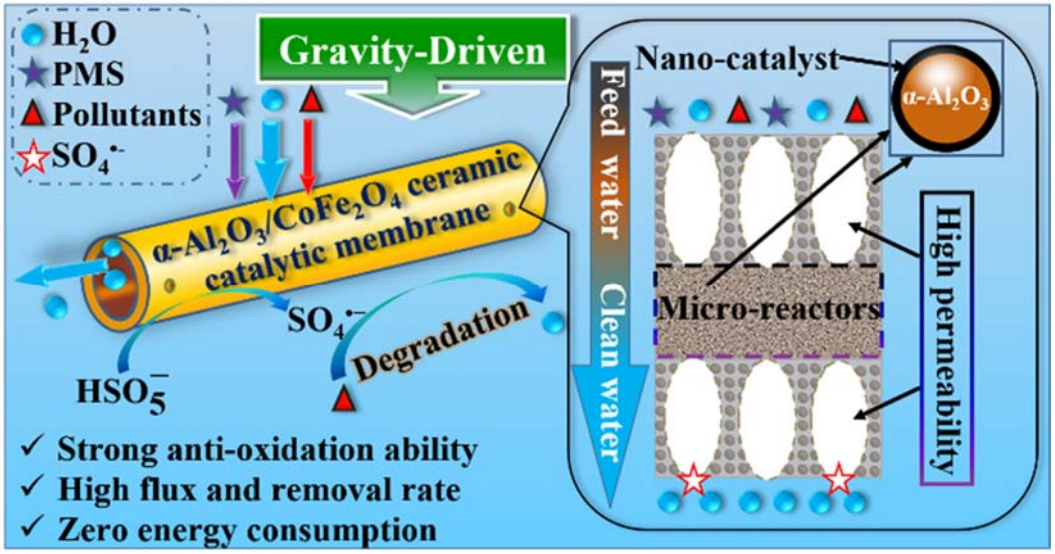

31

32

Abstract

Highly efficient water treatment is an important challenging issue for membrane separation where high flux, high removal rate, low fouling under low or even zero energy consumption are highly emphasized. In the present work, high-flux hierarchically structured ceramic membranes functionally decorated with active $CoFe_2O_4$ nano-catalyst was rationally designed and applied in highly efficient removal of emerging organic micro-pollutants from water. Coupling with sulfate radicals-advanced oxidation processes (SR-AOPs), such composite membranes could be operated with highly stable flux without any extra energy consumption, only under the gravity of the feeds, which is much more energy-efficient than traditional counterparts. After detailed structure characterizations, the performance such as flux, removal rate and stability were fully assessed. High flux can be attributed to the specially designed membrane structure with long finger-like macroporous layers featuring rapid transport, significantly outperforming other reported state-of-the-art separation membranes. High removal rate can be ascribed to a sponge-like layer loaded with nano-catalysts as micro-reactors for sufficient degradation of organic micro-pollutants. Mechanism analysis indicates that $SO_4^{\bullet-}$ is a dominant active radical responsible for catalytic degradation while physical adsorption played a minor effect. This technology is expected to be of potential for application in remote areas where power energy is absent, or simply used as a point-of-use technology in decentralized water treatment.

Keywords: Water treatment; Emerging micro-pollutants; Ceramic membrane; Nano-catalyst; High flux

1. Introduction

Rapid industrial development and urbanization result in dramatically increased discharge of various emerging contaminants such as organic dyes, pharmaceutical and personal care products (PPCPs), and endocrine disrupting compounds (EDCs) in wastewaters [1, 2]. Many of these compounds are of significant concerns due to their bioaccumulation, ecotoxicity and potential menace for human-beings, which calls for effective methods for their removal. Membrane separation, such as reverse osmosis (RO) [3] and nanofiltration (NF) [4, 5], can offer a wide-spectrum removal of various contaminants. However, under high operating pressure, RO and NF processes suffer from their high energy consumptions and low flux in spite of satisfactory removal rate. Like most membrane processes, their performance follows a permeability/selectivity trade-off [6]. In addition, these processes merely concentrate the contaminants, still leading to membrane fouling and secondary pollution in the form of brines. Thus, development of novel membrane separation technique featuring high permeability and low or even zero energy consumption with complete removal rate is still a challenging issue [7-11].

Advanced oxidation processes (AOPs) are able to efficiently degrade and mineralize recalcitrant organic pollutants from water [12]. To overcome the issues of catalyst recovery, many researchers immobilize their catalysts onto porous membranes to achieve simultaneous separation and catalytical removal of refractory contaminants [13]. For such catalytic membranes, robust ceramic supports are generally preferred over their polymeric counterparts due to their much better structural and chemical stability (particularly anti-oxidation ability) [14, 15]. In addition, ceramic substrates

also offer outstanding mechanical stability, thermal stability, anti-swelling ability and long life time [16-18].

Herein we report an advanced gravity-driven α-Al_2O_3/$CoFe_2O_4$ catalytic ceramic membrane coupling *in-situ* catalytic oxidation degradation with membrane separation for removal of emerging organic micro-pollutants from water. Different from traditional membrane structure, a hollow fiber membrane with hierarchical pore structure, which is comprised of a sponge-like layer sandwiched between two finger-like layers, was specially designed. The highly porous long finger-like micro-voids were used to minimize the hydraulic resistance and thereby to enable water rapidly transport under gravity-driven conditions with zero energy consumption. At the same time, the sponge-like layer was used to provide sufficient surfaces areas for incorporating $CoFe_2O_4$ nano-catalysts through a simple impregnation technique. In the presence of peroxymonosulfate (PMS), these nano-catalysts generate $SO_4^{\bullet-}$ radicals *in situ* [19], which have high standard reduction potential (2.5 – 3.1 V) [20], long half-life period (30-40 μs) [21] and broad applicable pH range (pH 2 – 8) [22, 23].

In this study, the pore structure, morphology, and formation of $CoFe_2O_4$ nano-catalysts of the α-Al_2O_3/$CoFe_2O_4$ catalytic ceramic membranes were systematically investigated. Without energy consumption, micro-pollutant model methyl blue (MB) and real micro-pollutant ibuprofen (low concentration in water) were used and their removal by the gravity-driven catalytic membrane was studied under various operational conditions to verify the feasibility. A degradation path mechanism was finally proposed to probe the catalytic function of true active radical species while adsorption kinetic of micro-pollutant molecular was also studied. The unique

hierarchical sandwich pore structure of the catalytic membrane resulted in highly efficient removal of the contaminants with ultra-high flux, significantly outperforming other reported state-of-the-art catalytic separation membranes, traditional RO and NF membranes. Our study provides a simple, effective and promising point-of-use membrane technology for decentralized water treatment especially where power energy is absent.

2. Material and methods

2.1. Materials and chemicals

Raw materials for preparation of α-Al_2O_3 membrane, α-Al_2O_3/$CoFe_2O_4$ catalytic ceramic membrane and reagents used in performance study are shown in Table S1. All the reagents were used as received and all solution prepared with reagents using ultrapure water from a GWA-UN pure water system.

2.2. Preparation of α-Al_2O_3/$CoFe_2O_4$ catalytic ceramic membrane

Hollow fiber α-Al_2O_3 membranes featuring sponge-like region and finger-like macro-voids were prepared by the phase inversion and sintering techniques (Text S2) according to the previous report [17, 24-26]. The special spinnerette with outer/inner diameter of 2.5 /1.3 mm was made by our laboratory in order to obtain ceramic membranes with low thickness. An impregnation technique combined with low temperature calcination process was applied to prepare α-Al_2O_3/$CoFe_2O_4$ catalytic ceramic membrane (Text S3). The $CoFe_2O_4$ catalyst mother solution was prepared via a soft chemistry method [27]. Specifically, 10 mmol $Co(NO_3)_3 \cdot 6H_2O$ and 20 mmol $Fe(NO_3)_3 \cdot 9H_2O$ were dissolved in 50 mL ultrapure water, and the obtained mixture

124 solution was added drop by drop into another 50 mL ultrapure water containing 30
125 mmol citric acid under vigorous stirring. After reaction at 60°C for 1 h, the solution was
126 cooled down to room temperature (22°C). The α-Al_2O_3 ceramic membranes were
127 dipped into the mother solution in a vertical direction, then soaked for 15 s, and finally
128 drawn out vertically at a speed of 3 $cm \cdot s^{-1}$. This coated membrane was dried in an oven
129 at 60°C for 1 h. These coating procedures can be repeated in cycles to control the
130 loading amount of $CoFe_2O_4$ nano-catalysts. Finally, the dried coated membranes were
131 calcined in a temperature programmable furnace. During calcination, the temperature
132 was increased to a target temperature (300°C, 400°C, 500°C) with a heating rate of
133 2°C·min^{-1} and a dwelling time of 120 min, before being cooled down naturally to the
134 room temperature (22°C).

135 **2.3. Characterizations**

136 The particle size distribution of α-Al_2O_3 was measured on a laser particle size
137 analyzer (Mastersizer 2000, Malvern Instruments Ltd., UK). X-ray diffraction (XRD)
138 pattern analysis was recorded using X-ray powder diffractometer (D/Max-2400) at 40
139 kV and 100 mA for monochromatized Cu K (=1.5418 Å) radiation. The pore size of
140 both ceramic substrates and catalytic membranes was tested under the pressure ranging
141 from 0 to 8.0 bar in a capillary flow porometer (Porolux 1000, Porometer NV, Germany)
142 based on gas-liquid displacement method. Scanning electron microscopy (SEM) and
143 energy dispersive X-ray (EDX) analyses were utilized to characterize the morphology
144 and micro-regional composition of the α-Al_2O_3 membranes and α-Al_2O_3/$CoFe_2O_4$
145 catalytic ceramic membranes using a FEI Quanta 450 system. Transmission electron
146 microscopy (TEM) and selected area electron diffraction (SAED) analyses were
147 conducted on a FEI Tecnai 20 Electron Microscope operated at 200 KV. Thermal

analysis of green membrane sample was determined by TG-DTA (TG/DTA 6300, Seiko co., Ltd). X-ray photoelectron spectroscopy (XPS) analysis was performed on a photoelectron spectrometer ECSALAB 250Xi with Al Kα (1486.6 ev) as the X-ray source. Fourier-transform infrared spectroscopy (FTIR) analysis was conducted on EQUINOX55 in the range of 4000-400 cm^{-1}. Streaming potential changes on membrane surface were conducted on an Electro Kinetic Analyzer (EKA) equipped with an asymmetric clamping cell (Anton Paar, Graz, Austria). MB and ibuprofen adsorption capacity were respectively characterized by quartz crystal microbalance (QCM, QCM E4, Biolin Scientitic) with an Au-coated resonator using 5 μL 0.05 wt.% PVC (polyvinyl chloride) DMF (N, N-Dimethylformamide) solutions. Electron paramagnetic resonance (EPR, Bruker, Germany) was used to analyze the $SO_4^{\bullet-}$ trapped with spin trapping agent 5,5-dimenthyl-1-pyrroline N-oxide (DMPO, > 99 wt.%). Zeta potentials on membrane surface at different pH values were conducted on a zeta potential analyzer (SurPASS 3, Anton paar, Austria). The degradation intermediates of MB and ibuprofen in the separation and catalyst system were identified by liquid chromatography-mass spectrometry (LC-MS, RRLC/6410B, Agilent, USA).

2.4. Catalytic-separation coupling process and mechanism analysis

Removal experiments of MB and ibuprofen were performed in a home-made gravity driven membrane system (Text S4, Figure S17) at room temperature (22°C). In order to effectively reduce membrane fouling, higher PMS dosage was used [28]. In a typical removal of MB, the length of catalytic ceramic membrane was 8 ± 0.1 cm. The ceramic membrane was first immersed into the experiment concentration of MB solution without adding PMS for 30 minutes to get an adsorption and desorption equilibrium. PMS (1.0 $g \cdot L^{-1}$) was added with certain volumes only once before running membrane

separation process since we in advance evaluated the total amount of consumed PMS. Then, the α-Al_2O_3/$CoFe_2O_4$ catalytic ceramic membrane was fixed inside a gravity driven membrane module, where water column height could be precisely adjustable. At given time intervals, permeate was collected with records of with weight and volume. The absorbance of the permeate was measured by using a UV-Vis spectrophotometer (UV-1100, Shanghai mapada Instruments) at 600 nm immediately when the sample was collected. The hydraulic retention time (*HRT*) was calculated according to Eq. 1, where V_m is the effective volume, δ is the apparent porosity (~46%) of the membrane, F is the average flow rate across the membrane at certain water column height.

$$HRT = \frac{V_m \cdot \delta}{F} \times 100\% \quad (1)$$

The removal of MB was calculated according to Eq. 2 [29], where A_0 is the absorbance of MB with initial concentration without any adjustment, A_t is the absorbance of MB after treatment for a specific time in the membrane system.

$$R\% = \frac{A_0 - A_t}{A_0} \times 100\% \quad (2)$$

The removal of ibuprofen was carried out according to the stated above with a little modification. 0.1 mL $NaNO_2$ (100 mM) was added to the permeate collected at the predetermined time to quench the radical reaction. The collected sample was kept at 4°C fridge and analyzed in 24 h. The concentration of ibuprofen was tested by using a HPLC system (Shimadzu, Japan, LC-10 AT) with a C18 reverse phase column (250 mm × 4.6 mm, 5 μm). The mobile phase consisted of acetonitril (HPLC grade) and 0.3% acetic acid (HPLC grade), water (70/30, volume ratio) with a flow rate of 0.4 $mL \cdot min^{-1}$ and an injection volume of 20 μL, and the excitation wavelength of 220 nm was used

for UV detection. Besides, the concentration of leached cobalt was conducted and analyzed on ICP-MS (Nex ION 300D, USA). All experiments were duplicated.

The optimized operation conditions during gravity driven process were determined by conducting 4-group control experiments including water column height, dosage of PMS, initial pH and initial MB concentration. According to the procedure as reported in elsewhere with minor modification, α-Al_2O_3/$CoFe_2O_4$ catalytic ceramic membrane was regenerated by impregnating it into 0.1 wt% NaOH solution, ultrapure water and ultrasonic with frequency of 60 Hz for 10 min repeatedly [15].

3. Results and discussion

3.1. Characterization of catalytic ceramic membranes

The ceramic membranes with controllable structure morphology consisting of adjustable sponge-like region and finger-like macro-voids could be rationally designed and prepared (Figure S1-S9, Table S2), which is an efficient way to prepare asymmetric membrane in one step. Figure 1a shows the digital photograph of the optimized hollow fiber α-Al_2O_3 membrane with an inserted cross-sectional SEM image. This membrane has an average pore size of 267.5 nm (Table S3). SEM images (Figures 1a, 1b) show that this membrane had a sandwiched structure, containing outer- and inner-layers featured with long finger-like macro-voids together with a sponge-like interlayer in between. The thickness of the outer-, inter-, and inner-layers were 161 ± 4, 111 ± 3, and 142 ± 3 μm, respectively, leading to an overall membrane thickness of approximately 420 ± 40 μm. This low thickness is approximately an order of magnitude lower than those of typical disc or tubular commercial α-Al_2O_3 membranes (~ 3 – 5 mm). In addition, the outer and inner layers together accounted for ~ 72% of the overall

membrane thickness. The combined small overall thickness and the sandwich structure resulted in a pure water permeability as high as 2633.7 $L \cdot m^{-2} \cdot h^{-1} \cdot bar^{-1}$, which was approximately 3 times of that for a commercial α-Al_2O_3 membranes with similar pore size (Figure 1c and Table S3). This extremely high water permeability enables the permeation of water only by its own gravity (e.g., under a water column height of 20 – 50 cm in the current study).

The sponge-like interlayer was characterized with smaller sized pores and more tortuous pore structure than finger-like regions (Figure S11). The impregnation-coating of $CoFe_2O_4$ nano-catalyst led to a very slight decrease of only 2.2% in pure water flux (Figure 1c and Table S3). The membrane structure was not significantly altered by the catalyst loading (Figure 1d, 1e). Detailed comparison showed greater presence of $CoFe_2O_4$ nano-catalyst in the sponge-like layer than long finger-like macro-voids (Figure 1f and Figure S11), which reveals the critical role of the sponge-like interlayer for the catalyst loading. This result can be explained by the mass transfer in the sandwich-structured membrane, with the cobalt-containing mother solution retained for longer time in the sponge-like interlayer due to its smaller and more tortuous pores. Such a special interlayer structure not only provides the majority of mechanical strength [24, 30], but also facilitates sufficient contact reaction between micro-pollutants and $SO_4^{\bullet-}$ generated from PMS catalyzed by $CoFe_2O_4$ nano-catalyst to significantly enhance degradation performance. Moreover, the uniform distribution of $CoFe_2O_4$ nano-catalysts was confirmed in the different structures of α-Al_2O_3 ceramic membranes such as inner/outer finger-like macro-voids (Figures S11d and S11f), intermediate sponge-like layer (Figure S11e) and membrane surface (Figure S15).

Interestingly, with increasing calcination temperature from 300°C to 500°C, the catalytic activities of α-Al_2O_3/$CoFe_2O_4$ catalytic ceramic membrane decreased (see the decreased removal rate of MB in Figure S12c) due to a decrease in the yield of sulfate radicals produced by catalyzing PMS. Low temperature calcination of $CoFe_2O_4$ nano-catalyst to form composite membrane is not only more beneficial for enhanced removal rate, but also enables lower energy consumption for membrane fabrication. In the current study, the best performance was achieved at a calcination temperature of 300°C (with $CoFe_2O_4$ crystal size of 8.2 nm), which is consistent with a previous study [27], was used throughout the rest of this study.

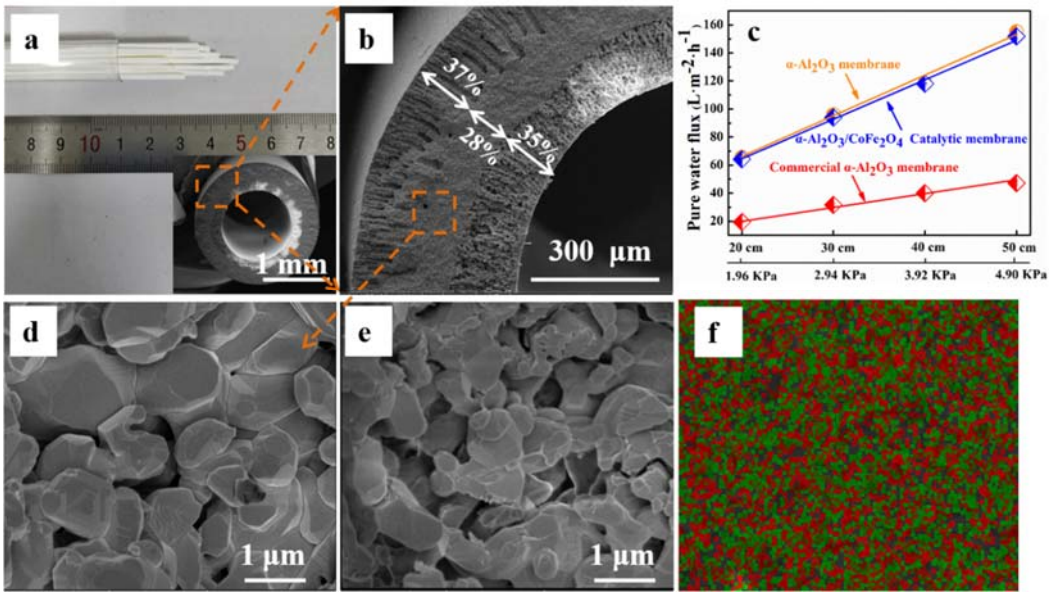

Figure 1. Digital photograph (a) and cross-sectional SEM image (inset of a), and locally enlarged cross-sectional SEM image (b) of α-Al_2O_3 membrane. Pure water flux (c) of α-Al_2O_3 membrane before and after impregnation-coating of $CoFe_2O_4$ nano-catalyst compared with commercial tubular alumina membrane. SEM image (d) of spongy-like layer of α-Al_2O_3 membrane. SEM image (e) and EDX mapping (f) of spongy-like layer of α-Al_2O_3/$CoFe_2O_4$ catalytic membrane calcined at 300°C. Fe signal, green; Co signal, red.

255 The loading amount of $CoFe_2O_4$ nano-catalysts can be steadily controlled via
256 selecting coating cycles (Figures S13 and S14). A very thin layer (~ 70 nm) of $CoFe_2O_4$
257 spinel nano-catalyst uniformly distributed on the surfaces of alumina particles, was
258 fully confirmed by some well-correlated characterizations such as SEM-EDX (Figures
259 S11 and S15), XRD (Figure S12a), FTIR (Figure S16), low-resolution TEM (Figures
260 2a and 2b), high-resolution TEM (Figure 2c), SAED pattern (Figure 2d) and XPS
261 (Figures 2e-2g). A brightness contrast difference was found within $CoFe_2O_4$ layer,
262 indicating that it consists of $CoFe_2O_4$ nano-crystals with increased specific surface area
263 (Figures 2a and 2b). The crystal structure of $CoFe_2O_4$ nano-catalyst is further revealed
264 by high-resolution TEM (Figure 2c). The lattice fringes with d-spacing values of 0.25
265 nm and 0.49 nm can be assigned to the (311) and (111) reflections of $CoFe_2O_4$ (Figure
266 2c), respectively [31]. Moreover, five concentric diffraction rings were observed in
267 SAED results (Figure 2d), which can be assigned to the (220), (311), (400), (511) and
268 (440) reflections of cubic $CoFe_2O_4$ nano-catalyst, respectively. The TEM results are in
269 good accordance with the results of XRD (Figure S12a). Figure 2e exhibits the XPS
270 peaks in the survey scan spectra of the surface of α-Al_2O_3/$CoFe_2O_4$ catalytic membrane,
271 which belongs to Al 2p, C 1s, O 1s, Fe 2p and Co 2p, respectively. Four peaks are
272 shown in the de-convolution of Co 2p peak (Figure 2f). The peak at 780.27 eV comes
273 from the Co2p3/2, while the peak at 796.12 eV arises from Co2p1/2. The satellite peaks
274 at around 786.31 eV and 802.84 eV belong to two shake-up type peaks of Co at the
275 high binding energy side of the Co2p3/2 and Co2p1/2 edges. The main and shake-up
276 satellite peaks of Co2p3/2 and Co2p1/2 indicate the presence of Co^{2+} in a high-spin
277 state [32]. The peaks at 710.96 eV and 724.6 eV comes from Fe2p3/2 and Fe2p1/2
278 respectively [33], indicating the presence of Fe^{3+} cation. All these results fully confirm

that $CoFe_2O_4$ nano-catalyst was formed on the surface of partially sintered alumina grains.

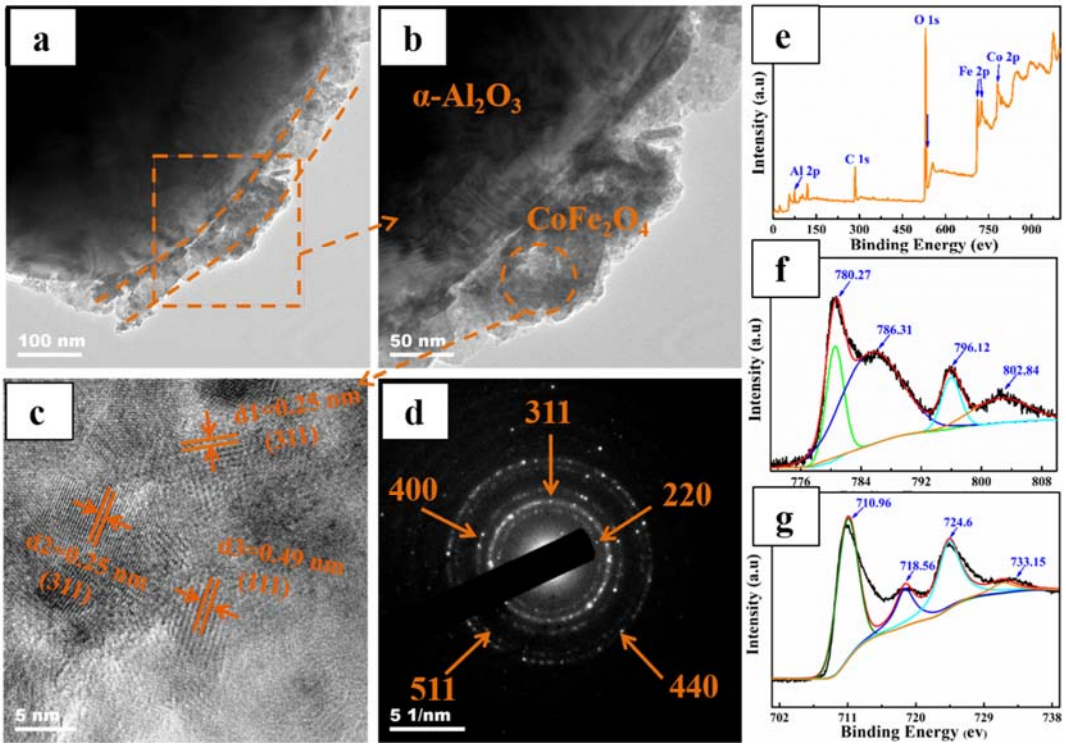

Figure 2. TEM images (a and b, low-resolution TEM; c, high-resolution TEM; d, SAED pattern) and XPS spectra (e, the survey spectrum; f, high resolution spectrum of Co element; g, high resolution spectrum of Fe element) of α-Al_2O_3/$CoFe_2O_4$ catalytic membrane calcined at 300°C.

3.2. Performance of α-Al_2O_3/$CoFe_2O_4$ catalytic ceramic membrane

Figure 3 presents the MB removal performance of α-Al_2O_3/$CoFe_2O_4$ catalytic membrane under various conditions with the gravity of the feed as driving force. Compared to pristine α-Al_2O_3 membrane and α-Al_2O_3/$CoFe_2O_4$ catalytic membrane without PMS, the α-Al_2O_3/$CoFe_2O_4$ catalytic membrane with the presence of PMS possessed much higher removal rates for MB (89.9% ~ 98.6%) (Figure 3a) under a stable normalized flux, indicating very weak membrane fouling (Figure 3b) [34, 35].

Compared to α-Al_2O_3 membrane, α-Al_2O_3/$CoFe_2O_4$ catalytic membranes showed much higher sorption capacity of MB molecular due to the existence of $CoFe_2O_4$ nano-catalysts. QCM results showed much higher sorption of MB of α-Al_2O_3/$CoFe_2O_4$ catalytic membranes compared to α-Al_2O_3 membrane (Figure 3c). Therefore, removal pathway of MB using α-Al_2O_3/$CoFe_2O_4$ catalytic membrane probably includes surface adsorption and radical catalytic degradation. When the feed water that contains MB and PMS passed through the α-Al_2O_3/$CoFe_2O_4$ catalytic membrane, the $CoFe_2O_4$ nano-catalyst decorated within the membrane reacted with PMS to produce $SO_4^{\bullet-}$, which is an active radical with a strong ability to oxidize MB for degradation. Specifically, as shown in Figure 1b, the sponge-like layer provided sufficient contact area between PMS and $CoFe_2O_4$ nano-catalyst for generation of more $SO_4^{\bullet-}$, thus between $SO_4^{\bullet-}$ and pollutant molecules for rapid degradation, facilitating the significant enhancement of removal rate.

Figures 3d-3g present the separation performance of α-Al_2O_3/$CoFe_2O_4$ catalytic membrane at different operation conditions. The α-Al_2O_3/$CoFe_2O_4$ catalytic membrane had noticeable removal of MB under water column heights of 20 – 50 cm (Figure 3d). An obvious discoloration was observed for permeate (the inset of Figure 3d, with a feed concentration of 25 ppm MB). At a low water column height of 20 cm, high average removal rate of ~ 98% was maintained. Remove rate decreased as water column weight increased (Figure 3d). High water column height resulted in a relatively high trans-membrane pressure, shortening the retention time of MB pollutants within the α-Al_2O_3/$CoFe_2O_4$ catalytic membrane and thus causing an incomplete reaction between radicals and pollutants. Meanwhile, at lower water column height, more stable water flux was maintained (Figure S18a). This reduced membrane fouling tendency is

316 consistent with the better catalytical removal of MB by the produced radicals due to
317 longer retention-reaction time at low water column heights [36]. With decreasing water
318 column height from 50 to 20 cm (i.e., increasing HRT from 4.1 to 9.3 s), higher MB
319 removal efficiency was achieved. In our experiments, with water column height
320 increased, the removal rate decreased (Figure 3d) while the water flux increased (Figure
321 1c, Figure S18a). This indicates that a trade-off relationship exists between removal
322 rate and water flux under different water column heights. Considering this trade-off
323 issue between water flux and removal rate, 30 cm was chosen as the final water column
324 height in the following experiments. Furthermore, a well-fitted exponentially
325 decreasing relationship between water column height and MB residual percentage was
326 observed at different operation times (Figure 3h). The results imply that water column
327 height imparts an important influence on removal rate of MB for the α-Al_2O_3/$CoFe_2O_4$
328 catalytic membrane coupling with sulfate radicals-advanced oxidation processes (SR-
329 AOPs). Thus, the efficient removal of pollutants could be accomplished via reasonably
330 controlling water column height.

331 The effects of the dosage of PMS, initial pH and MB concentration were further
332 investigated. A significant increase of removal rate was observed when the PMS dosage
333 increased in the range of 0.0 – 4.0 $g \cdot L^{-1}$. At a dosage level of 1.0 $g \cdot L^{-1}$, the average
334 removal rate maintained above 91.8%. However when the dosage of PMS increased
335 from 2.0 $g \cdot L^{-1}$ to 4.0 $g \cdot L^{-1}$, the removal rate increased slightly (Figure 3e). The
336 phenomenon could be attributed to 1) the scavenge of $SO_4^{\bullet-}$ by excess HSO_5^- to form
337 a less reactive $SO_5^{\bullet-}$ species (Eq. 2) [37]; and 2) the formation of unreactive $S_2O_8^{2-}$
338 species at high concentrations of PMS (Eq. 3) [38]. Although high PMS dosage has a

better performance in removing MB, considering its dosage cost and performance, 1.0 $g \cdot L^{-1}$ was considered as the optimum in the following experiments.

$$SO_4^{\bullet -} + HSO_5^- \rightarrow SO_5^{\bullet -} + SO_4^{2-} + H^+ \quad (2)$$

$$SO_4^{\bullet -} + SO_4^{\bullet -} \rightarrow S_2O_8^{2-} \quad (3)$$

Figure 3f displays the variations of removal rate of MB with operation time using α-$Al_2O_3/CoFe_2O_4$ catalytic membrane under different initial pH values. With pH increasing from 2.85 to 9.00, the removal rate of MB decreased. According to the *pK*a values of PMS ($pKa_1 < 0$ and $pKa_2 = 9.4$) [33, 39], PMS mainly exists as the form of HSO_5^- over the pH range of 2.85 to 9.0, resulting in a high catalytic efficiency. With pH increasing, the different electrostatic repulsion and the surface absorbance of $CoFe_2O_4$ nano-catalyst influence the removal of MB together. However, when the initial pH increased up to 11, removal rate decreases due to surface absorbance. In this case, •OH became a dominant radical while scavenging of $SO_4^{\bullet -}$ resulted in lower oxidation efficiency [23].

With increasing MB concentration, the removal rate decreased especially from 50 to 100 $mg \cdot L^{-1}$ (Figure 3g). The average removal rates were 91.8%, 91.2% and 56% for initial concentration 25 $mg \cdot L^{-1}$, 50 $mg \cdot L^{-1}$, and 100 $mg \cdot L^{-1}$, respectively. However, no obvious difference in removal rate was observed from 25 $mg \cdot L^{-1}$ to 50 $mg \cdot L^{-1}$, suggesting a good application potential. This phenomenon is attributed to the effective reaction between $SO_4^{\bullet -}$ and MB with low concentration in the gravity-driven membrane process.

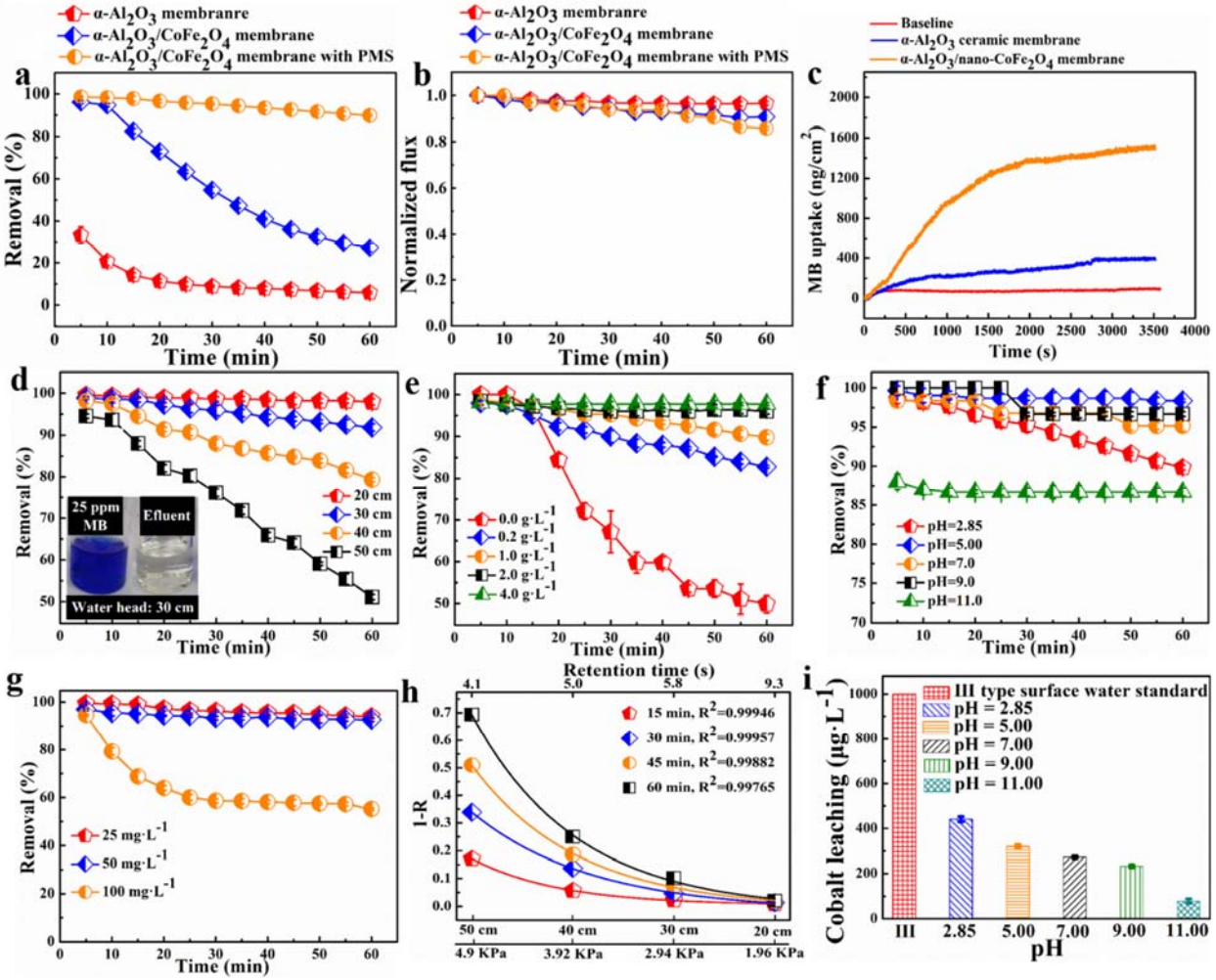

360 **Figure 3.** Removal rate (a) and normalized flux (b) of α-Al_2O_3/$CoFe_2O_4$ catalytic membrane *in-situ*
361 coupling SR-AOPs for MB removal and degradation in water. MB adsorption behavior test (c) of
362 α-Al_2O_3/$CoFe_2O_4$ catalytic membrane and α-Al_2O_3 membrane by QCM. Effects of different
363 parameters on the removal rate of MB: (d) water column height, ([MB] = 25 mg·L^{-1}, pH = 2.85,
364 [PMS] = 1.0 g·L^{-1}, membrane length = 8.0 ± 0.1 cm); (e) PMS dosage, ([MB] = 25 mg·L^{-1}, H = 30
365 cm, pH = 2.85, membrane length = 8.0 ± 0.1 cm); (f) initial pH, ([MB] = 25 mg·L^{-1}, H = 30 cm,
366 [PMS] = 1.0 g·L^{-1}, membrane length = 8.0 ± 0.1 cm); (g) concentration of simulated MB, ([PMS] =
367 1.0 g·L^{-1}, H = 30 cm, pH = 2.85, membrane length = 8.0 ± 0.1 cm). (h) The relationship between
368 MB residual ratio and water column height, where R is the removal rate of MB, and 1-R represents
369 for the residual ratio of MB in the effluent. Conditions: [MB] = 25.0 mg·L^{-1}, [PMS] = 1.0 g·L^{-1}, T
370 = 22°C, membrane length = 8.0 ± 0.1 cm, without adjustment of pH. (i) Concentration of leached

cobalt ions in the permeate at different initial pH (from 2.85 to 11). Conditions: [MB] = 25 $mg \cdot L^{-1}$, H = 30 cm, [PMS] = 1.0 $g \cdot L^{-1}$, membrane length = 8.0 ± 0.1 cm.

The concentration of leached cobalt ions in the permeate was measured for environment risk assessment as shown in Figure 3i. It decreased with increasing pH value from 2.85 to 11. The concentrations of leached cobalt ions are all lower than that (662 $\mu g \cdot L^{-1}$) reported previously [40] and China III type surface water standard [41], indicating that the α-Al_2O_3/$CoFe_2O_4$ catalytic membrane is both effective and environment friendly.

Besides MB, the α-Al_2O_3/$CoFe_2O_4$ catalytic membrane was also quite effective for highly efficient removal of ibuprofen. As shown in Figures 4a and 4b, the α-Al_2O_3/$CoFe_2O_4$ catalytic membrane coupling with SR-AOPs possessed much higher removal rates for ibuprofen (~ 99.5%), and also exhibited an almost complete removal of ibuprofen at a stable normalized flux with very weak membrane fouling. Compared with MB (Figure 3c), higher removal rate of ibuprofen can be attributed to the weaker adsorption on the membrane surface as clearly observed in the QCM result (Figure 4c). More importantly, α-Al_2O_3/$CoFe_2O_4$ catalytic membrane had extremely high water permeability of 2575 $L \cdot m^{-2} \cdot h^{-1} \cdot bar^{-1}$ (Figure 4d and Table S3), significantly outperforming other existing state-of-the-art membranes such as other catalytic membranes, traditional RO and NF membranes.

This feature enabled the membrane developed in the current study to be driven with zero energy consumption only by the gravity of feed at a trans-membrane pressure as low as ~ 0.02 bar while maintaining high removal rate of MB (95 ~ 98%) and ibuprofen (~ 99.5%). The membrane system with high flux and rejection without any extra energy

consumption is promising for highly efficient treatment of wastewaters containing persistent organic contaminants. Besides high flux and removal rate, the α-Al_2O_3/$CoFe_2O_4$ catalytic membrane developed in our work possesses a good reusability and durability (Figure S19).

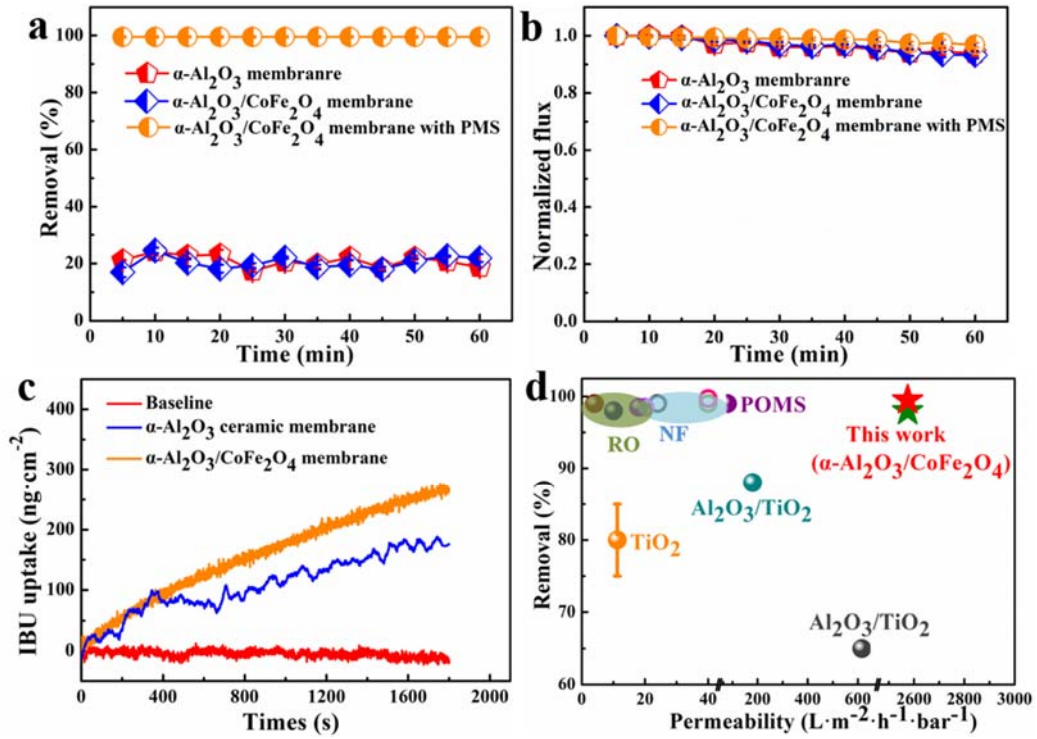

Figure 4. Removal rate (a) and normalized flux (b) of α-Al_2O_3/$CoFe_2O_4$ catalytic membrane *in-situ* coupling SR-AOPs for ibuprofen removal and degradation in water. Operation conditions: [Ibuprofen] = 2.0 mg·L^{-1}, [PMS] = 1.0 g·L^{-1}, T = 22°C, water column height = 30.0 cm, membrane length = 8.0 ± 0.1 cm, without adjustment of pH. (c) Ibuprofen adsorption behavior test of α-Al_2O_3/$CoFe_2O_4$ catalytic membrane and α-Al_2O_3 membrane by QCM. (d) Comparison of water permeability and removal rate between α-Al_2O_3/$CoFe_2O_4$ catalytic membrane fabricated in the current study and other existing catalytic membranes [29, 42-47], traditional RO [48-50] and NF membranes [5, 51-53].

3.3. Mechanism analysis

Membrane surface streaming potential test can be used to reveal surface charge change on time during removal of micro-pollutants in water [54]. The higher potential difference, the stronger the adsorption ability. As shown in Figures 5a and 5b, when the amount of adsorbed MB achieved equilibrium, the streaming potential difference was 5.2 mV and 42.3 mV for α-Al_2O_3 membrane and α-Al_2O_3/$CoFe_2O_4$ catalytic membrane, respectively. Therefore, the adsorption of MB on membrane surface plays a non-negligible (but minor) role in micro-pollutant removal especially for α-Al_2O_3/$CoFe_2O_4$ catalytic membrane, which also has a much higher absorption ability than α-Al_2O_3 membrane.

In order to identify the dominant radical responsible for micro-pollutant catalytic degradation, radical quenching experiments were carried out by using tert-butyl alcohol (TBA) and ethanol as the quenching molecular probes because their reaction rate with $SO_4^{\bullet-}$ and •OH differs significantly. The second reaction rate constants of TBA are (4.0 ~ 9.4)×10^5 $M^{-1}\cdot S^{-1}$ and (3.8 ~ 7.6)×10^8 $M^{-1}\cdot S^{-1}$ with $SO_4^{\bullet-}$ and •OH, respectively, while the second reaction rate constants of EtOH are (1.6 ~ 7.7) ×10^7 $M^{-1}\cdot S^{-1}$ with $SO_4^{\bullet-}$, and (1.2 ~ 2.8) ×10^9 $M^{-1}\cdot S^{-1}$ with •OH [55]. As shown in Figure 5c, there is almost no difference in removal rate with time for the membrane systems with (removal rate-91.3%, the blue curve) and without (removal rate-91.8%, the yellow curve) addition of 1.0 M TBA, indicating that •OH was not the dominant radical in catalytic degradation of MB in the systems. However, the removal rate of MB significantly decreased from 91.8% to 81.5% with the presence of 1.0 M EtOH (the red curve). This is attributed to the fact that EtOH mainly consumed $SO_4^{\bullet-}$, thus inhibiting the removal rate of MB. The results indicated that $SO_4^{\bullet-}$ is the dominant radical for micro-pollutant catalytic degradation. As shown in Figure 5d, EPR results demonstrates that $SO_4^{\bullet-}$ was steadily

produced by $CoFe_2O_4$ nano-catalyst and PMS. Acidic condition was more favorable for the production of more $SO_4^{\bullet-}$. The results agree well with the removal rate at different pH values shown in Figure 3f.

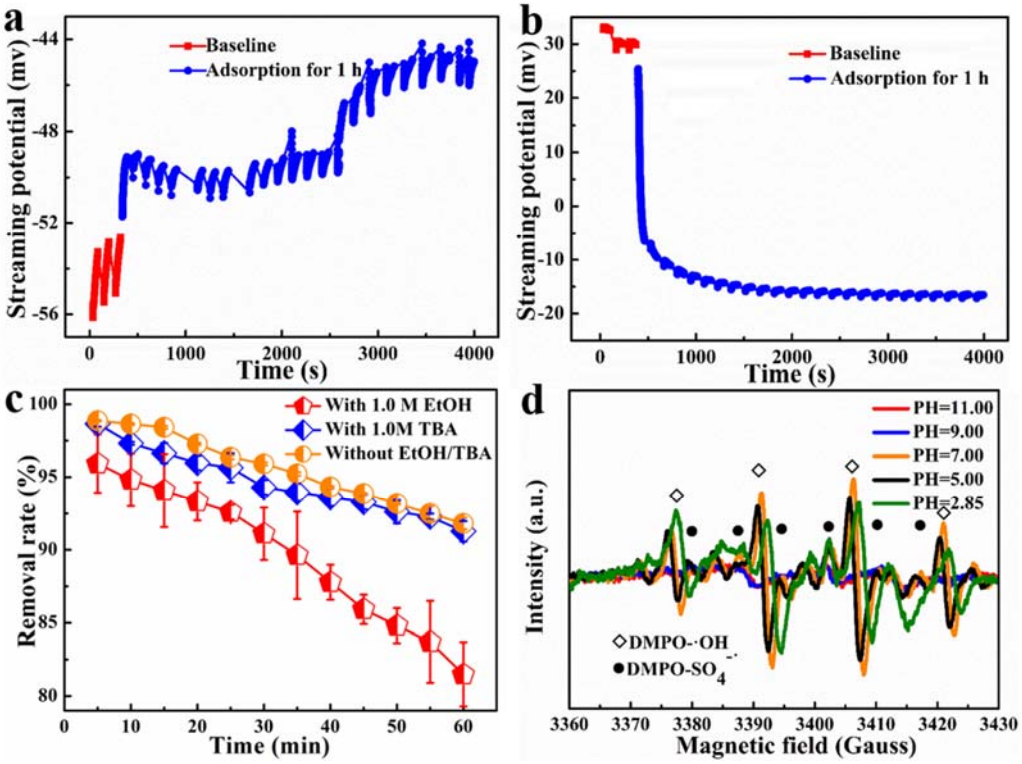

Figure 5. The streaming potential of α-Al_2O_3 membrane (a) and α-Al_2O_3/$CoFe_2O_4$ catalytic membrane (b) under test conditions: [MB] = 25 mg·L^{-1}, [KCl] = 1.0 mmol·L^{-1}, pH = 6.85, room temperature (22°C), N_2 surrounding, P = 250 mbar; (c) radical quenching experiment, conditions: [MB] = 25 mg·L^{-1}, [PMS] = 1.0 g·L^{-1}, H = 30 cm, membrane length = 8.0 ± 0.1 cm, pH without adjustment (pH = 2.9), room temperature (22°C), (d) EPR results at different pH value.

To further reveal the degradation mechanism with intermediates formed during the process, the permeation solutions were analyzed by LC-MS. The discussion of ESI-MS spectra obtained in this work was related to *m/z* values assigned to different compounds presented in Figure S20 and Figure S21. The reaction processes of $CoFe_2O_4$ inducing PMS are shown in Eq. 4 – Eq. 7 [28], with $SO_4^{\bullet-}$, •OH, OH^- and the possible

intermediates. In $CoFe_2O_4$ nano-catalyst, actually Co presented a valent state of +2 (left side in Eq. 4) before reaction. Indeed, this can be supported by the XPS analysis of α-Al_2O_3/$CoFe_2O_4$ catalytic membrane, indicating that only Co^{2+} was detected (Figure 2e, 2f). However, Co^{2+} then partially underwent an increase from +2 to +3 in valent state after catalytic reaction (right side in Eq. 4). Coupled with the results in Figure 5, $SO_4^{\bullet-}$ was likely the dominant radical in the catalytic degradation process. Based on the above results, the degradation process mechanism of MB and ibuprofen is proposed in Figure 6.

$$\equiv Co^{2+} + HSO_5^- \rightarrow \equiv Co^{3+} + SO_4^{\bullet-} + OH^- \quad (4)$$

$$SO_4^{\bullet-} + OH^- \rightarrow SO_4^{2-} + \bullet OH \quad (5)$$

$$\equiv Co^{3+} + HSO_5^- \rightarrow \equiv Co^{2+} + SO_5^{\bullet-} + H_2O \quad (6)$$

$$SO_5^{\bullet-} + O_2^- \rightarrow SO_4^{\bullet-} + O_2 \quad (7)$$

$$SO_4^{\bullet-} + \text{MB/Ibuprofen} \rightarrow \text{Organic intermediates} + CO_2 + H_2O \quad (8)$$

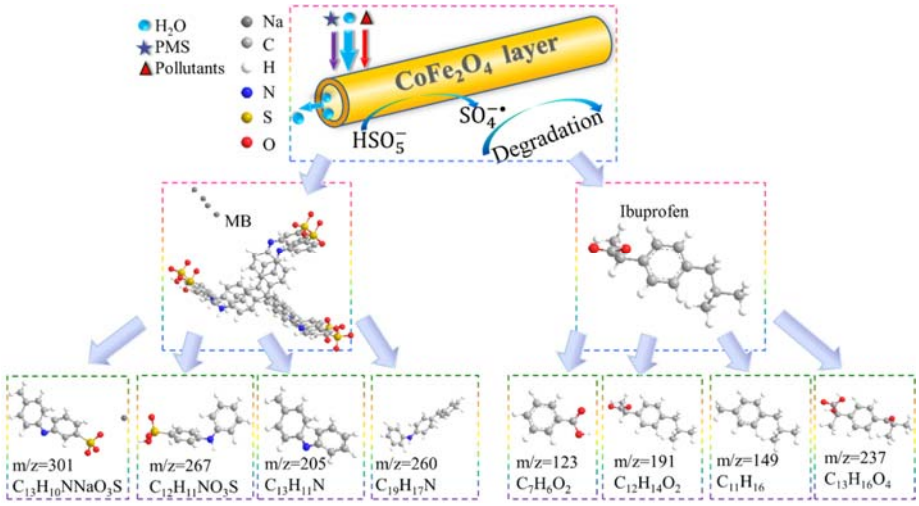

Figure 6. Degradation pathways for MB and ibuprofen in the membrane separation and catalytic process.

4. Conclusions

In this work, a rationally structural design strategy for development of zero energy consumption and high performance robust catalytic ceramic membrane was presented for highly efficient removal of emerging organic micro-pollutants in wastewater. To overcome the key issues of conventional membrane separation (e.g., high energy consumption, low flux and membrane fouling), we designed a sandwiched α-Al_2O_3/$CoFe_2O_4$ catalytic ceramic membrane structure highly efficient coupling membrane separation with catalytic degradation, which exhibits a great potential for removal of MB and ibuprofen. The finger-like macropores ensures high water permeability (2575 $L \cdot m^{-2} \cdot h^{-1} \cdot bar^{-1}$) to allow the rapid permeation of water only under its gravity without any extra energy input, significantly outperforming other reported state-of-the-art separation membranes such as traditional RO and NF membranes with lower performance which still needs much higher energy consumption. Active $CoFe_2O_4$ nano-catalysts loaded in the sponge-like interlayer acts as efficient micro-reactors to not only effectively degrade organic contaminants but also significantly minimize membrane fouling. A very low leaching level of cobalt ions was also observed, indicating no environment risk for water treatment. Coating of nano-catalyst indeed increased the adsorption of micro-pollutants on membrane surface, but played a minor role on removal performance. Both removal efficiency and water flux could be maintained at relatively high levels. Considering the toxicity of sulfate ions above a certain level, their removal will be studied via employing post-treatment methods such as nanofiltration and reverse osmosis in our follow-up study. Also the toxicity assessment of intermediates after catalytic degradation is being under way as a follow-up study. By employing the same protocol, the design strategy for catalytic ceramic

membranes can be directly extended to other membrane systems with different ceramic substrates (such as zirconia, mullite and spinel) and other active MFe_2O_4 (M = Cu, Ni, Zn, Mn) nano-catalysts. Such membranes, with the promising features such as better performance in permeability and removal efficiency but zero energy consumption, can be also employed for removal of other organic micro-pollutants from various water streams. Our study provides a potential platform for the development of low energy consumption and high efficiency robust membranes for highly efficient removal of various emerging micro-pollutants.

Acknowledgments

This work was financially supported by the Youth Top-Notch Talent Program of Talent Project of Revitalizing Liaoning (No. XLYC1807250), National Natural Science Foundation of China (No. 21876020), National Key Research and Development Project (No. 2019YFA0705803), the Fundamental Research Funds for the Central Universities (No. DUT19LAB03), the Haitian Scholar Program from Dalian University of Technology and the 111 Program of Introducing Talents of Discipline to Universities (No. B13012).

Appendix A. Supplementary data

Details and descriptions of experimental methods (Figure S3, Table S2 and Figure S17). Results and discussions on the characterization of raw materials (Figure S1 and Figure S2), fabrication, optimization and characterization of α-Al_2O_3 membrane (Figure S4, Figure S5, Figure S6, Figure S7, Figure S8 and Figure S9) and α-Al_2O_3/ $CoFe_2O_4$ catalytic membrane (Figure S10, Figure S11, Figure S12, Figure 13, Figure

509 S14, Figure S15 and Figure S16), as well as performance for α-Al_2O_3/$CoFe_2O_4$ catalytic

510 membrane (Figure S18, Figure S19, Figure S20 and Figure S21).

Reference

[1] F. Chen, A.S. Gong, M. Zhu, G. Chen, S.D. Lacey, F. Jiang, Y. Li, Y. Wang, J. Dai, Y. Yao, J. Song, B. Liu, K. Fu, S. Das, L. Hu, Mesoporous, three-dimensional wood membrane decorated with nanoparticles for highly efficient water treatment, ACS Nano, 11 (2017) 4275-4282.

[2] S.R. Hughes, P. Kay, L.E. Brown, Global synthesis and critical evaluation of pharmaceutical data sets collected from river systems, Environ. Sci. Technol., 47 (2013) 661-677.

[3] J. Liu, Z. Wang, C.Y. Tang, J.O. Leckie, Modeling dynamics of colloidal fouling of RO/NF membranes with a novel collision-attachment approach, Environ. Sci. Technol., 52 (2018) 1471-1478.

[4] Z. Yang, Z.W. Zhou, H. Guo, Z. Yao, X.H. Ma, X. Song, S.P. Feng, C.Y. Tang, Tannic Acid/Fe^{3+} nanoscaffold for interfacial polymerization: toward enhanced nanofiltration performance, Environ. Sci. Technol., 52 (2018) 9341-9349.

[5] H. Guo, L.E. Peng, Z. Yao, Z. Yang, X. Ma, C.Y. Tang, Non-polyamide based nanofiltration membranes using green metal-organic coordination complexes: implications for the removal of trace organic contaminants, Environ. Sci. Technol., 53 (2019) 2688-2694.

[6] H.B. Park, J. Kamcev, L.M. Robeson, M. Elimelech, B.D. Freeman, Maximizing the right stuff: The trade-off between membrane permeability and selectivity, Science, 356 (2017) eaab0530.

[7] H. Huang, K. Schwab, J.G. Jacangelo, Pretreatment for low pressure membranes in water pretreatment-A review, Environ. Sci. Technol., 43 (2009) 3011-3019.

534 [8] X. Cheng, H. Liang, A. Ding, X. Tang, B. Liu, X. Zhu, Z. Gan, D. Wu, G. Li,
535 Ferrous iron/peroxymonosulfate oxidation as a pretreatment for ceramic
536 ultrafiltration membrane: Control of natural organic matter fouling and degradation
537 of atrazine, Water Res., 113 (2017) 32-41.
538 [9] M.A. Shannon, P.W. Bohn, M. Elimelech, J.G. Georgiadis, B.J. Marinas, A.M.
539 Mayes, Science and technology for water purification in the coming decades,
540 Nature, 452 (2008) 301-310.
541 [10] J.R. Werber, C.O. Osuji, M. Elimelech, Materials for next-generation desalination
542 and water purification membranes, Nat. Rev. Mater., 1 (2016).
543 [11] J. Wang, H. Guo, Z. Yang, Y. Mei, C.Y. Tang, Gravity-driven catalytic
544 nanofibrous membranes prepared using a green template, J. Membr. Sci., 525 (2017)
545 298-303.
546 [12] N.N. Tušar, D. Maučec, M. Rangus, I. Arčon, M. Mazaj, M. Cotman, A. Pintar, V.
547 Kaučič, Manganese functionalized silicate nanoparticles as a Fenton-type catalyst
548 for water purification by advanced oxidation processes (AOP), Adv. Funct. Mater.,
549 22 (2012) 820-826.
550 [13] J. Zhang, H. Yu, X. Quan, S. Chen, Y. Zhang, Ceramic membrane separation
551 coupled with catalytic ozonation for tertiary treatment of dyestuff wastewater in a
552 pilot-scale study, Chem. Eng. J., 301 (2016) 19-26.
553 [14] Y. Guo, B. Xu, F. Qi, A novel ceramic membrane coated with MnO_2–Co_3O_4
554 nanoparticles catalytic ozonation for benzophenone-3 degradation in aqueous
555 solution: Fabrication, characterization and performance, Chem. Eng. J., 287 (2016)
556 381-389.

[15] M. Chen, L. Zhu, J. Chen, F. Yang, C.Y. Tang, M.D. Guiver, Y. Dong, Spinel-based ceramic membranes coupling solid sludge recycling with oily wastewater treatment, Water Res., 169 (2019) 115180.

[16] Y. Dong, L. Ma, C.Y. Tang, F. Yang, X. Quan, D. Jassby, M.J. Zaworotko, M.D. Guiver, Stable superhydrophobic ceramic-based carbon nanotube composite desalination membranes, Nano Lett., 58 (2018) 5514-5521.

[17] L. Li, M. Chen, Y. Dong, X. Dong, S. Cerneaux, S. Hampshire, J. Cao, L. Zhu, Z. Zhu, J. Liu, A low-cost alumina-mullite composite hollow fiber ceramic membrane fabricated via phase-inversion and sintering method, J. Eur. Ceram. Soc., 36 (2016) 2057-2066.

[18] M. Chen, L. Zhu, Y. Dong, L. Li, J. Liu, Waste-to-resource strategy to fabricate highly porous whisker-structured mullite ceramic membrane for simulated oil-in-water emulsion wastewater treatment, ACS Sustainable Chem. Eng., 4 (2016) 2098-2106.

[19] A. Rastogi, S.R. Al-Abed, D.D. Dionysiou, Effect of inorganic, synthetic and naturally occurring chelating agents on Fe(II) mediated advanced oxidation of chlorophenols, Water Res., 43 (2009) 684-694.

[20] T. Zhang, H. Zhu, J.P. Croue, Production of sulfate radical from peroxymonosulfate induced by a magnetically separable $CuFe_2O_4$ spinel in water: efficiency, stability, and mechanism, Environ. Sci. Technol., 47 (2013) 2784-2791.

[21] P. Hu, M. Long, Cobalt-catalyzed sulfate radical-based advanced oxidation: A review on heterogeneous catalysts and applications, Appl. Catal., B, 181 (2016) 103-117.

580 [22] R. Yuan, S.N. Ramjaun, Z. Wang, J. Liu, Effects of chloride ion on degradation of
581 acid orange 7 by sulfate radical-based advanced oxidation process: implications for
582 formation of chlorinated aromatic compounds, J. Hazard. Mater., 196 (2011) 173-
583 179.
584 [23] Y.F. Huang, Y.H. Huang, Identification of produced powerful radicals involved in
585 the mineralization of bisphenol A using a novel UV-$Na_2S_2O_8$/H_2O_2-Fe(II, III) two-
586 stage oxidation process, J. Hazard. Mater., 162 (2009) 1211-1216.
587 [24] L. Zhu, M. Chen, Y. Dong, C.Y. Tang, A. Huang, L. Li, A low-cost mullite-titania
588 composite ceramic hollow fiber microfiltration membrane for highly efficient
589 separation of oil-in-water emulsion, Water Res., 90 (2016) 277-285.
590 [25] B.F.K. Kingsbury, K. Li, A morphological study of ceramic hollow fibre
591 membranes, J. Membr. Sci., 328 (2009) 134-140.
592 [26] C.C. Wei, O.Y. Chen, Y. Liu, K. Li, Ceramic asymmetric hollow fibre membranes-
593 one step fabrication process, J. Membr. Sci., 320 (2008) 191-197.
594 [27] J. Deng, Y. Shao, N. Gao, C. Tan, S. Zhou, X. Hu, $CoFe_2O_4$ magnetic nanoparticles
595 as a highly active heterogeneous catalyst of oxone for the degradation of diclofenac
596 in water, J. Hazard. Mater., 262 (2013) 836-844.
597 [28] Y. Ren, L. Lin, J. Ma, J. Yang, J. Feng, Z. Fan, Sulfate radicals induced from
598 peroxymonosulfate by magnetic ferrospinel MFe_2O_4 (M = Co, Cu, Mn, and Zn) as
599 heterogeneous catalysts in the water, Appl. Catal., B, 165 (2015) 572-578.
600 [29] R. Li, Y. Jia, N. Bu, J. Wu, Q. Zhen, Photocatalytic degradation of methyl blue
601 using Fe_2O_3/TiO_2 composite ceramics, J. Alloys Compd., 643 (2015) 88-93.
602 [30] L. Zhu, X. Dong, M. Xu, F. Yang, M.D. Guiver, Y. Dong, Fabrication of mullite
603 ceramic-supported carbon nanotube composite membranes with enhanced

performance in direct separation of high-temperature emulsified oil droplets, J. Membr. Sci., 582 (2019) 140-150.

[31] L. Jing, Y. Xu, S. Huang, M. Xie, M. He, H. Xu, H. Li, Q. Zhang, Novel magnetic $CoFe_2O_4$/Ag/Ag_3VO_4 composites: Highly efficient visible light photocatalytic and antibacterial activity, Appl. Catal., B, 199 (2016) 11-22.

[32] W. Bian, Z. Yang, P. Strasser, R. Yang, A $CoFe_2O_4$/graphene nanohybrid as an efficient bi-functional electrocatalyst for oxygen reduction and oxygen evolution, J. Power Sources, 250 (2014) 196-203.

[33] C. Tan, N. Gao, D. Fu, J. Deng, L. Deng, Efficient degradation of paracetamol with nanoscaled magnetic $CoFe_2O_4$ and $MnFe_2O_4$ as a heterogeneous catalyst of peroxymonosulfate, Sep. Purif. Technol., 175 (2017) 47-57.

[34] D. Lu, T. Zhang, L. Gutierrez, J. Ma, J.P. Croue, Influence of surface properties of filtration-layer metal oxide on ceramic membrane fouling during ultrafiltration of oil/water emulsion, Environ. Sci. Technol., 50 (2016) 4668-4674.

[35] D.J. Miller, S. Kasemset, D.R. Paul, B.D. Freeman, Comparison of membrane fouling at constant flux and constant transmembrane pressure conditions, J. Membr. Sci., 454 (2014) 505-515.

[36] Z. He, D.J. Miller, S. Kasemset, D.R. Paul, B.D. Freeman, The effect of permeate flux on membrane fouling during microfiltration of oily water, J. Membr. Sci., 525 (2017) 25-34.

[37] J. Madhavan, P. Maruthamuthu, S. Murugesan, S. Anandan, Kinetic studies on visible light-assisted degradation of acid red 88 in presence of metal-ion coupled oxone reagent, Appl. Catal., B, 83 (2008) 8-14.

627 [38] C.L. Clifton, R.E. Huie, Rate constants for hydrogen abstraction reactions of the
628 sulfate radical, SO_4^{-}. Alcohols, Int. J. Chem. Kinet., 21 (1989) 677-687.
629 [39] Y. Feng, D. Wu, Y. Deng, T. Zhang, K. Shih, Sulfate radical-mediated degradation
630 of sulfadiazine by $CuFeO_2$ rhombohedral crystal-catalyzed peroxymonosulfate:
631 synergistic effects and mechanisms, Environ. Sci. Technol., 50 (2016) 3119-3127.
632 [40] Y. Du, W. Ma, P. Liu, B. Zou, J. Ma, Magnetic $CoFe_2O_4$ nanoparticles supported
633 on titanate nanotubes ($CoFe_2O_4$/TNTs) as a novel heterogeneous catalyst for
634 peroxymonosulfate activation and degradation of organic pollutants, J. Hazard.
635 Mater., 308 (2016) 58-66.
636 [41] GB3838-2002, Environmental quality standards for surface water, In Chinese.
637 [42] L. Yao, L. Zhang, R. Wang, S. Chou, Z. Dong, A new integrated approach for dye
638 removal from wastewater by polyoxometalates functionalized membranes, J.
639 Hazard. Mater., 301 (2016) 462-470.
640 [43] B. Zhu, Y. Hu, S. Kennedy, N. Milne, G. Morris, W. Jin, S. Gray, M. Duke, Dual
641 function filtration and catalytic breakdown of organic pollutants in wastewater
642 using ozonation with titania and alumina membranes, J. Membr. Sci., 378 (2011)
643 61-72.
644 [44] H. Zhang, X. Quan, S. Chen, H. Zhao, Y. Zhao, Fabrication of photocatalytic
645 membrane and evaluation its efficiency in removal of organic pollutants from water,
646 Sep. Purif. Technol., 50 (2006) 147-155.
647 [45] R.M. Huertas, M.C. Fraga, J.G. Crespo, V.J. Pereira, Sol-gel membrane
648 modification for enhanced photocatalytic activity, Sep. Purif. Technol., 180 (2017)
649 69-81.

650 [46] Y. Guo, Z. Song, B. Xu, Y. Li, F. Qi, J.P. Croue, D. Yuan, A novel catalytic
651 ceramic membrane fabricated with $CuMn_2O_4$ particles for emerging UV absorbers
652 degradation from aqueous and membrane fouling elimination, J. Hazard. Mater.,
653 344 (2018) 1229-1239.
654 [47] X. Cheng, D. Wu, H. Liang, X. Zhu, X. Tang, Z. Gan, J. Xing, X. Luo, G. Li,
655 Effect of sulfate radical-based oxidation pretreatments for mitigating ceramic UF
656 membrane fouling caused by algal extracellular organic matter, Water Res., 145
657 (2018) 39-49.
658 [48] R. Bernstein, S. Belfer, V. Freger, Toward improved boron removal in RO by
659 membrane modification: feasibility and challenges, Environ. Sci. Technol., 45
660 (2011) 3613-3620.
661 [49] Y. Yao, W. Zhang, Y. Du, M. Li, L. Wang, X. Zhang, Toward enhancing the
662 chlorine resistance of reverse osmosis membranes: an effective strategy via an end-
663 capping technology, Environ. Sci. Technol., 53 (2019) 1296-1304.
664 [50] N. Togo, K. Nakagawa, T. Shintani, T. Yoshioka, T. Takahashi, E. Kamio, H.
665 Matsuyama, Osmotically assisted reverse osmosis utilizing hollow fiber membrane
666 module for concentration process, Ind. Eng. Chem. Res., 58 (2019) 6721-6729.
667 [51] S. Li, J. Luo, X. Hang, S. Zhao, Y. Wan, Removal of polycyclic aromatic
668 hydrocarbons by nanofiltration membranes: Rejection and fouling mechanisms, J.
669 Membr. Sci., 582 (2019) 264-273.
670 [52] C. Tang, L. Jameso, Membrane independent limiting flux for RO and NF
671 membranes fouled by humic acid.pdf, Environ. Sci. Technol., 41 (2007) 4767-4773.

[53] C. Boo, Y. Wang, I. Zucker, Y. Choo, C.O. Osuji, M. Elimelech, High performance nanofiltration membrane for effective removal of perfluoroalkyl substances at high water recovery, Environ. Sci. Technol., 52 (2018) 7279-7288.

[54] K. Greben, P. Li, D. Mayer, A. Offenhausser, R. Wordenweber, Immobilization and surface functionalization of gold nanoparticles monitored via streaming current/potential measurements, J. Phys. Chem. B, 119 (2015) 5988-5994.

[55] G. Fang, W. Wu, C. Liu, D.D. Dionysiou, Y. Deng, D. Zhou, Activation of persulfate with vanadium species for PCBs degradation: A mechanistic study, Appl. Catal., B, 202 (2017) 1-11.